



Effect of laser energy density on bead characteristics in wire-DED

SUMITKUMAR RATHOR[✉], RAVI KANT^{*✉} and EKTA SINGLA[✉]

Department of Mechanical Engineering, Indian Institute of Technology Ropar, Rupnagar, Punjab 140001, India
e-mail: rathor.20mez0005@iitrpr.ac.in; rathorsumitkumar@gmail.com; ravi.kant@iitrpr.ac.in;
only4ravikant@gmail.com; ekta@iitrpr.ac.in; ekta.singla@gmail.com

MS received 25 September 2023; revised 4 December 2023; accepted 17 January 2024

Abstract. Achieving repeatability in part production remains a challenge in laser-wire feed directed energy deposition (LW-DED). It is necessary to understand the laser-wire deposition and bead aspect ratio varying the process conditions to achieve repeatability. Laser energy density is one of the key process parameters that affect the dimensions of the deposit. So, this study discusses the fundamentals of depositing the copper-coated ER70S-6 low carbon steel wire. The laser energy density effects on aspect ratio, overall porosity, microstructure, and microhardness are presented. The bead morphology changes with the change in laser energy density. Single track deposited sample results helped in understanding the melt transition for material deposition and dimensional resolution of the deposited track.

Keywords. Laser-wire; volumetric energy density; temperature; bead morphology; ER70S-6; porosity; additive manufacturing.

1. Introduction

Additive manufacturing (AM) has become increasingly popular in recent years due to its ability to produce complex geometries with good mechanical properties in the automobile and aerospace industries [1–5]. The three features of AM technologies are building complex geometries with high functionality, dimensional precision, and toolless manufacturing. Metal AM technologies are capable of fabricating metallic parts without additional manufacturing processes. The two leading technologies in metal AM are powder bed fusion (PBF) and directed energy deposition (DED) [6, 7]. PBF technology works based on utilizing powder particles to get fused by the effect of heat sources, like Laser and Electron beams [8]. The DED works by depositing material onto a substrate or surface by melting, where it solidifies to get the desired shape [9]. The feedstock material for DED technology can be wire or powder particles. Feedstock selection is based on material, machine, process conditions, work environment, and desired properties.

Wire-based DED systems are becoming popular because they have high deposition rates, build large parts, and use minimum support structures [10]. These processes lack the dimensional resolution to achieve detailed smaller size feature in a part. At the same time, it is beneficial in several applications that require the flexibility of manipulation provided by the system and increased dimensional

resolution using wire as a feedstock material. Recent applications identified in-space manufacturing, where powder management becomes difficult in less gravity. The popular processes are Wire-arc AM (WAAM) and Laser-wire feed DED. In traditional WAAM process, defects can arise from the high heat generated due to arc, causing problems such as extra heat input and heat affected zone [11]. So, it is a need to figure out a method that should control the heat input and build high geometrical resolution parts.

The laser-wire feed directed energy deposition (LW-DED) process has been used to deposit metal alloys using laser as a heat source [12]. The laser beam is highly focused due to its superior characteristics such as monochromaticity and coherence. Material deposition in LW-DED was achieved by considering process parameters such as laser power, spot diameter, and laser travel speed to calculate laser energy density. Key aspects of achieving high dimensional resolution were reported by only using thin wires and flexible manufacturing systems [13, 14]. Laser energy density can also be a key aspect in achieving high dimensional resolution with fewer defects. Energy densities are described as linear (J/mm), areal (J/mm²), and volumetric (J/mm³). The volumetric energy density will be more reliable as it considers the interdependencies of more process parameters.

In this study, the Fe-based ER70S-6 copper-coated wire is a depositing material to investigate bead morphology and other mechanical properties. It is challenging to deposit ER70S-6 material using laser as a heat source due to the

*For correspondence

presence of copper, a laser reflective material. This material is suitable for automatic welding and can achieve excellent welding properties, low sputter, high deposition efficiency, and low cost in the process [15, 16]. ER70S-6 material is widely studied in the literature using the WAAM process [17]. This work is the first attempt aimed at the fundamental understanding of the effect of volumetric laser energy density on bead morphology for depositing copper coated ER70S-6 material in a wire-DED process. This work carries detailed experimental work depicting the process capabilities regarding bead morphology, temperature analysis, microstructure evolution, and microstructure distribution of single track deposits.

2. Materials and methods

2.1 Materials

The substrate used was 4 mm thick regular mild steel as it has good weldability with ER70S-6 wire. The wire of ER70S-6 alloy with 1.2 mm diameter was purchased from Maruti Welding Wires, India, and it was used as received. Table 1 shows the chemical composition of the wire and substrate.

2.2 Experiment

The trials were conducted using an in-house developed LW-DED experimental setup shown in figure 1(a-b). The setup includes a 1000 W fibre laser source operating at a wavelength of 1080 nm. The wire feeder was also in-house developed and can feed wire diameters ranging from 0.5 to 1.2 mm. The unidirectional deposition strategy was used to deposit the tracks with 10 mm hatch spacing adjacently. An infrared (IR) camera (A315, FLIR, SWEDEN) recorded the track melt pool temperature during the trials. The camera was placed at approximately 0.5 m and 45° angles from the substrate. The processing parameters are presented in table 2.

2.3 Characterization

The deposited samples were cut, mounted, and polished to study the heat-affected zone (HAZ) depth and microstructure of the deposits after etching with a 5% Nital-Nitric and

Ethanol solution. Olympus GX53 light optical microscope was used for HAZ and microstructural analysis. The HAZ depth was measured using images captured by an optical microscope. The area of change in microstructures was considered to determine the HAZ depth. The microstructure analysis was done on the specimen extracted from the single tracks for each energy density. Micro-hardness test was performed using Vickers indenter (WILSON 402MVD) with a load of 100 g, spacing of 400 μm, and 10 s dwell time per indentation. A total of 30 indentations per sample were taken and reported. The beads were cut from the substrate, and porosity was determined using the Archimedes approach [18]. Each sample was measured three times, and the result was recorded when the scale reached equilibrium. The density of deposited tracks (ρ_{sample}) was measured using the density meter with an accuracy of 0.001 g/cm³ and following Eq. (1). The mass in the air (M_{air}) and mass in the fluid (M_{fluid}) were measured for each sample. Here, ρ_{fluid} is the density of the fluid and ρ_{air} is the density of the air. The porosity is calculated using Eq. (2).

$$\rho_{\text{sample}} = \frac{M_{\text{air}}}{M_{\text{air}} - M_{\text{fluid}}} * (\rho_{\text{fluid}} - \rho_{\text{air}}) + \rho_{\text{air}} \quad (1)$$

$$\% \text{Porosity} = 100 - \left(\frac{\rho_{\text{sample}} * 100}{\rho_{\text{theoretical}}} \right) \quad (2)$$

3. Results and discussion

3.1 Single track characterization

The morphology of the layers and dimensional measurements of single tracks are influenced by metallurgical properties in additive manufacturing. The dimensional characteristics of the laser-wire deposition were evaluated to see the effect of deposition parameters [19].

Laser energy density

$$= \frac{\text{Laser power (W)}}{\text{Laser spot area (mm}^2\text{)} \times \text{print speed (mm/s)}} \text{J/mm}^3 \quad (3)$$

The deposition tracks can be seen in figure 2(a), the range of energy density is from 20 to 32 J/mm³, calculated using Eq. (3). All the investigated cases, except 20 J/mm³ energy density, continuous single tracks were observed with varying widths. A change in width and discontinuity was observed as energy density increased from 20 and 24 J/mm³. However, as energy density increased to 32 J/mm³, there was an increase in the track width (2.69 mm). This change occurred because of lower energy density supplied at shorter laser-material interaction times. This led to less heat penetrating the base plate. Heat-affected zone depth

Table 1. Chemical composition (wt.%) of the wire and substrate used for this study.

Elements	C	Mn	Si	S	P	Cu	Fe
ER70S-6	0.15	1.85	1.15	0.035	0.025	0.50	Bal.
Mild Steel	0.16	0.70	0.40	0.04	0.04	–	Bal.

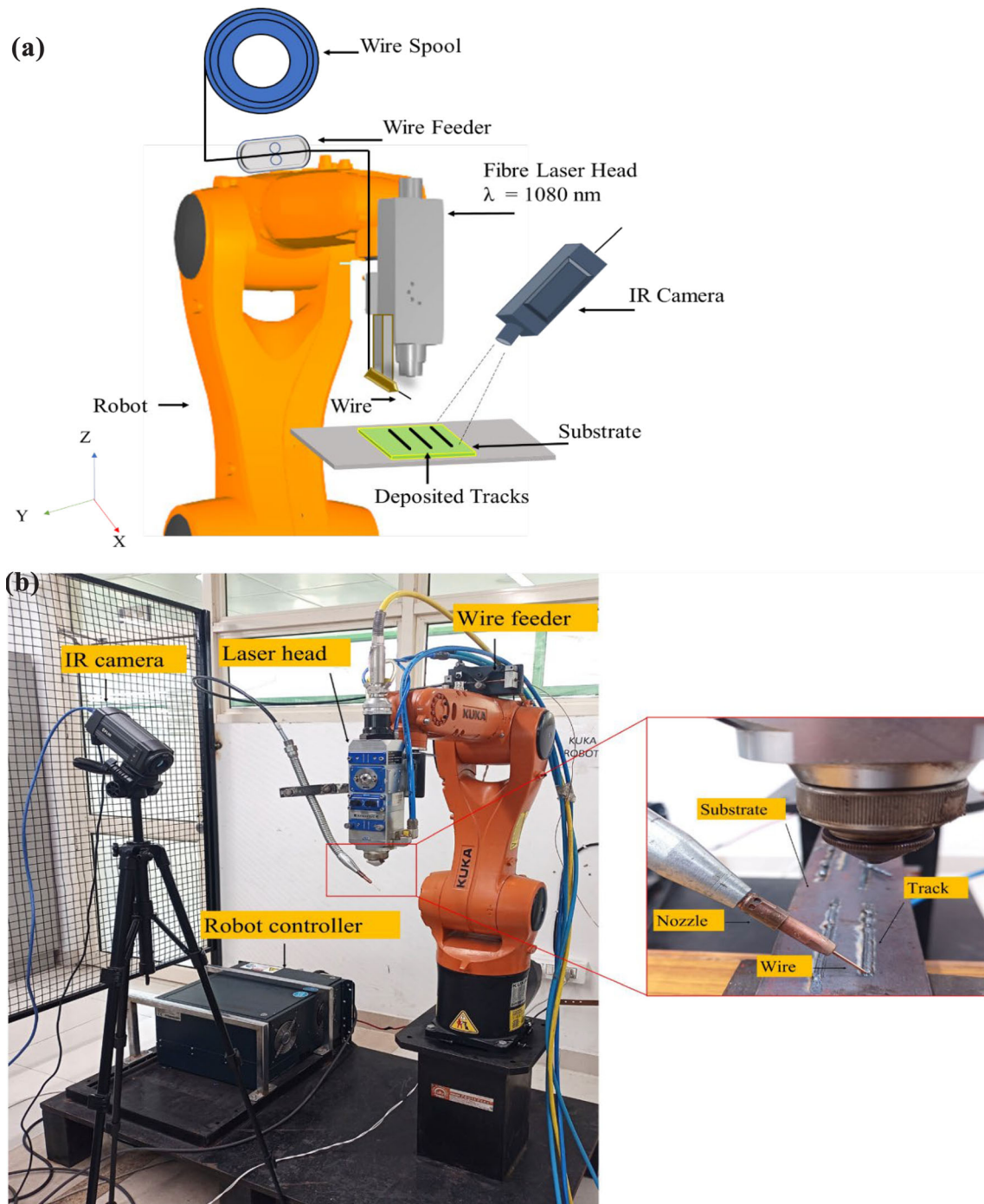


Figure 1. (a) Schematic of in-house developed LW-DED experimental setup and (b) Robotic LW-DED experimental setup used in this study.

Table 2. Processing parameter of LW-DED process.

Parameters	Value
Laser power	500, 600, 700, 800 W
Laser energy density	20, 24, 28, 32 J/mm ³
Track length	100 mm
Wire feed rate	13 mm/s
Deposition speed	2 mm/s
Beam diameter	4 mm

can also confirm the heat penetration, as it increases with energy density.

The single tracks were characterized to determine the changes in melt characteristics with energy density. The results are presented in figure 2(b) and plotted as a function of laser energy density in figure 3(a-b). The wettability of the material on the base plate was characterized by the melt pool depth. Further, the bead height and HAZ depth were

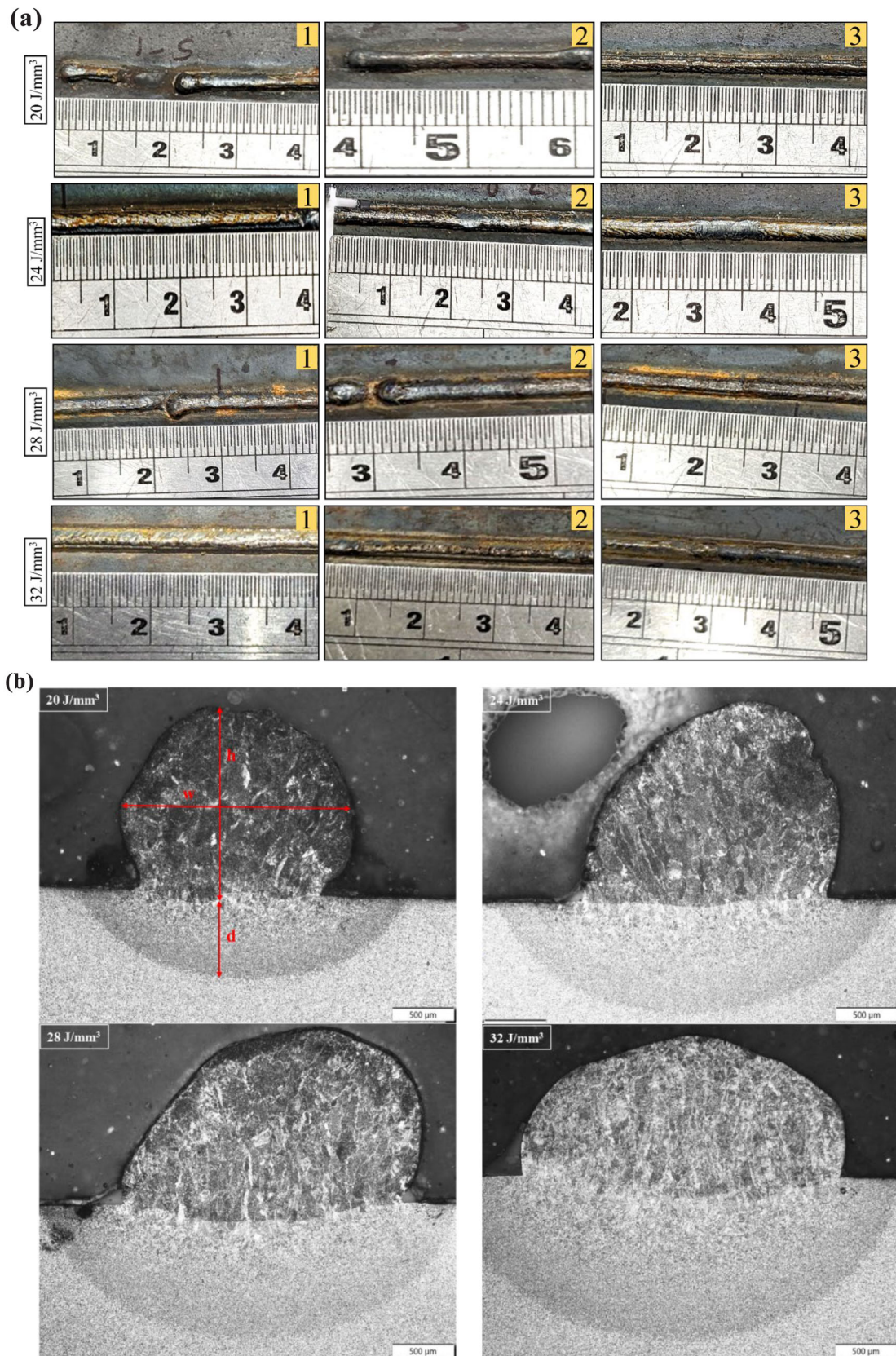


Figure 2. (a) Single track images of ER70S-6 at the different energy density and (b) Cross section of single track of ER70S-6 after etching at varying energy density.

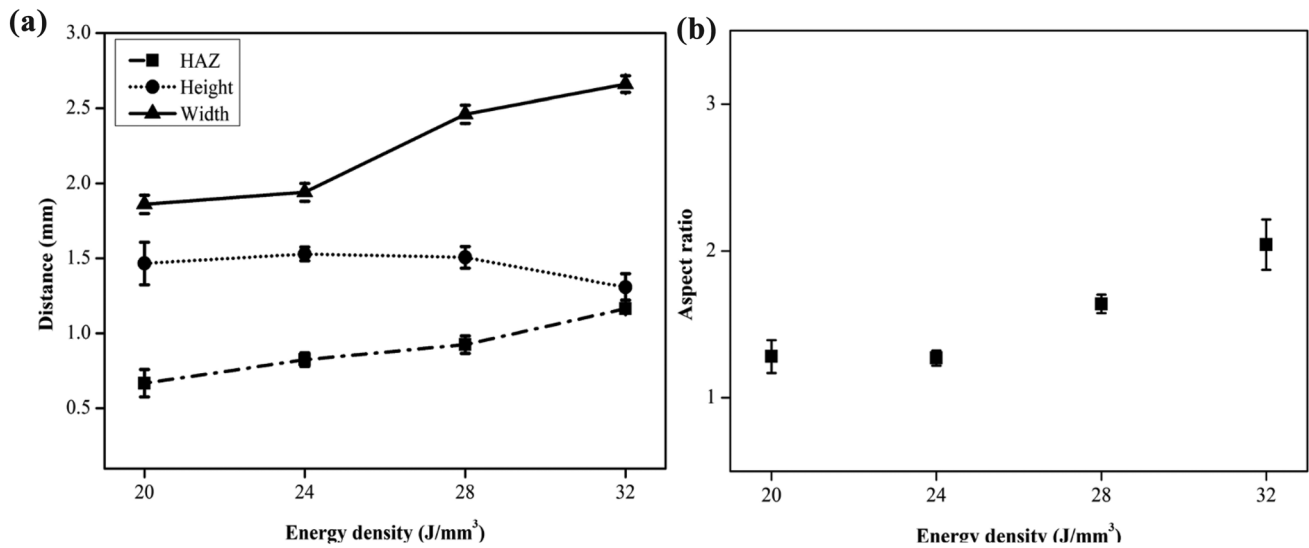


Figure 3. (a) Dimensions of single track width and bead height as a function of laser energy density and (b) Aspect ratio as a function of laser energy density.

measured to determine the ideal parameters for this material. The melt pool depth values are 0.07 mm, 0.1 mm, 0.13 mm, and 0.19 mm for energy density values 20, 24, 28, and 32 J/mm^3 , respectively.

It shows that higher energy density values will result in deeper penetration into the substrate. The track width increased from 1.92 to 2.69 mm as energy density increased. Increased intensity of the laser causes higher width, resulting in a large volume of melting, wider beads, and deeper melt pool [20]. The bead analysis depicted that higher energy would influence the bead structure with a high aspect ratio. The single tracks dimensions were measured using ImageJ software (10 readings per sample) for the images obtained using an optical microscope and plotted against the energy density presented in figure 3(a). At higher energy density, the width of the bead was spotted higher, whereas it was observed less at lower energy density. The trend for bead height shows less variation with change in energy density.

The aspect ratio of the beads was measured using the width-to-height ratio. A higher aspect ratio will be ideal for overlap during AM to ensure the track with minimum porosity. At higher energy density, melt pool shape drastically changes and can cause ‘keyhole’ shaped pores between layers, causing defects [21, 22]. Due to lower energy density, less energy penetration into depositing material was observed, and the substrate caused balling effect due to liquid metal surface tension [23].

The two major types of porosity in the additive manufacturing of metals are interlayer and intralayer porosity. The interlayer porosity occurs due to insufficient energy to melt deposit material. Intralayer pores are due to gas entrapment, a ‘keyhole’ defect. The minimum porosity was observed at 24 J/mm^3 and increases as laser energy density

increases. Laser energy density is correlated with dilution. High dilution indicates the occurrence of intralayer porosities. A lower value of laser energy density led to less dilution (the negative slope), denoting the possibility of a fusion defect. The higher values of laser energy density led to dilution (the positive slope), denoting a higher possibility of forming keyhole porosity [24].

3.2 Temperature analysis

The IR thermal imaging camera was used to provide the temperature reading of the upper surface of the depositing weld bead during the process. Yadav *et al* [25] determined the emissivity of mild steel, the temperature is measured using a thermocouple and recorded by a data acquisition system. The thermal imaging camera maps this temperature measurement with a thermocouple and estimates the emissivity, which typically ranges from 0.7 to 0.72. For this study, an emissivity of 0.71 was used. The location for laser-wire interaction can be seen at figure 4(a) and Sp1, Sp2, and Sp3 are taken at the center of the track and are presented in figure 4(b). The continuous temperature distribution along the track length when the laser was at three different spot positions, Sp1, Sp2, and Sp3 recorded and presented in figure 4(c). It was observed that the variation of maximum temperature measured at different energy densities is close to the melting temperature of the material. The high temperature at the melt pool is reaching at peak without delay. It can be due to the laser absorbed in the deposition interface and the high thermal conductivity of wire and substrate material.

The flames were observed at the start of the deposition tracks, i.e., Sp1. Some temperature peaks showed disturbances at the first spot due to flame formation and

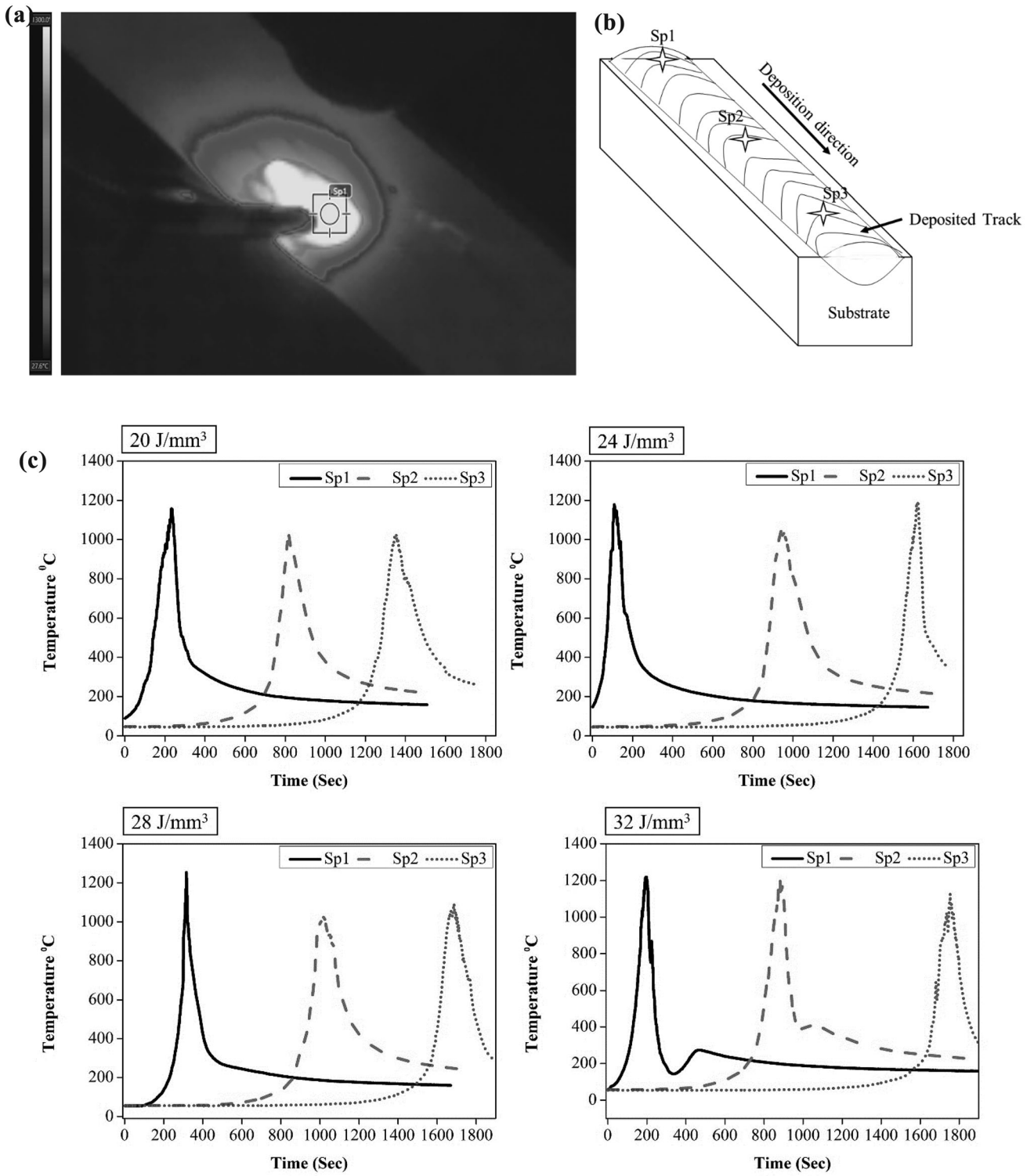


Figure 4. (a) IR measurement of melt pool temperature of ER70S-6 at Sp1, (b) Schematic showing locations of Sp1, Sp2, and Sp3 on the track and (c) The melt pool temperature with time for different spot positions showing increase in temperature at the start of the track and then approximately same on other positions

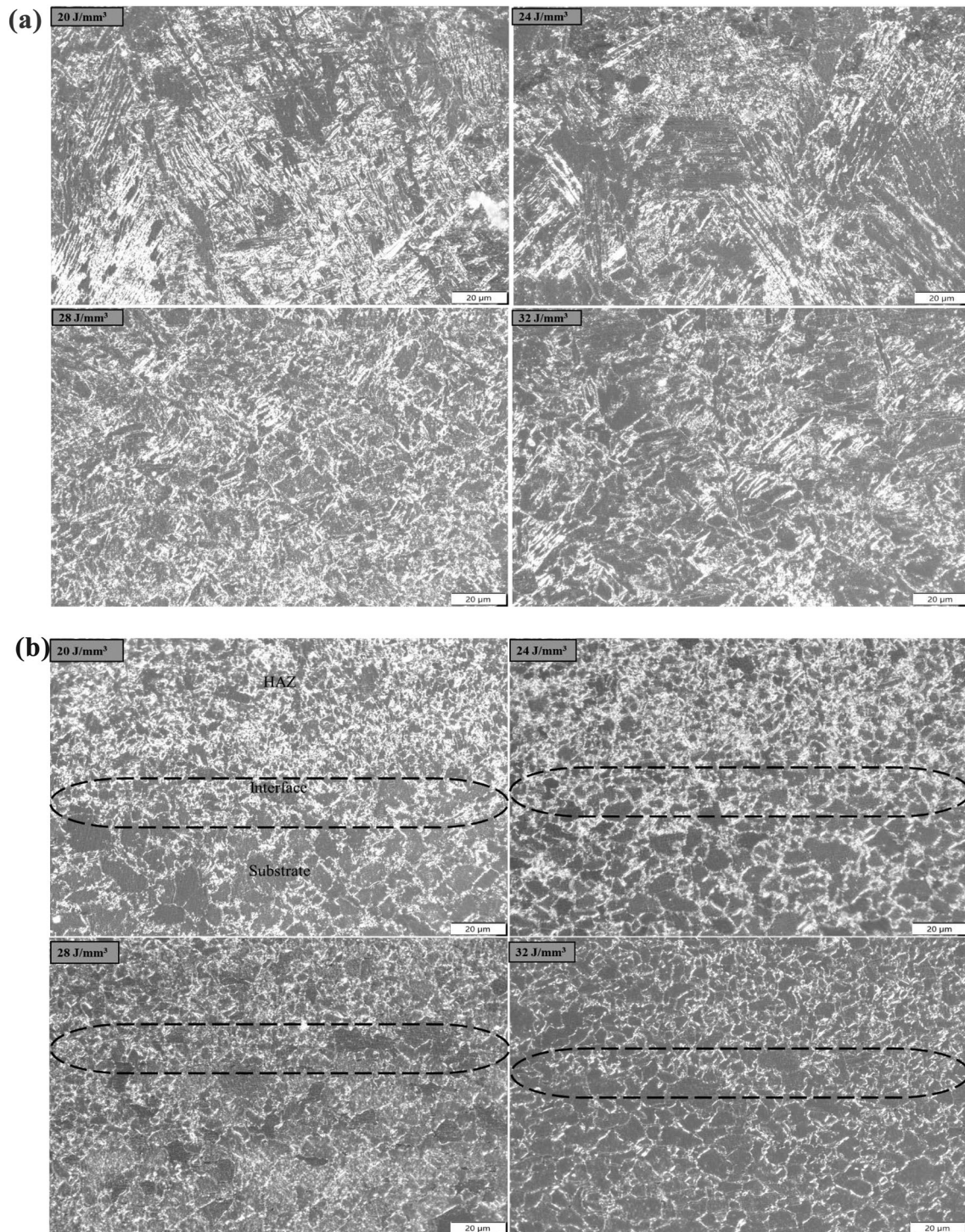


Figure 5. (a) Micrographs of deposited bead showing the elongated grains and it reduces with increase in laser energy density and (b) Micrographs of interface at substrate and HAZ.

irregularities in both materials during the laser-material interaction. The laser spot position affects the temperature in the interaction zone. The laser diameter covered the wire more than two times its diameter to form a uniform bead. It

was observed for 32 J/mm³ energy density that the temperature peaks are more uniform throughout the track; hence, the more uniform bead was observed after deposition. The laser-wire interaction was for a short time (μ s) in

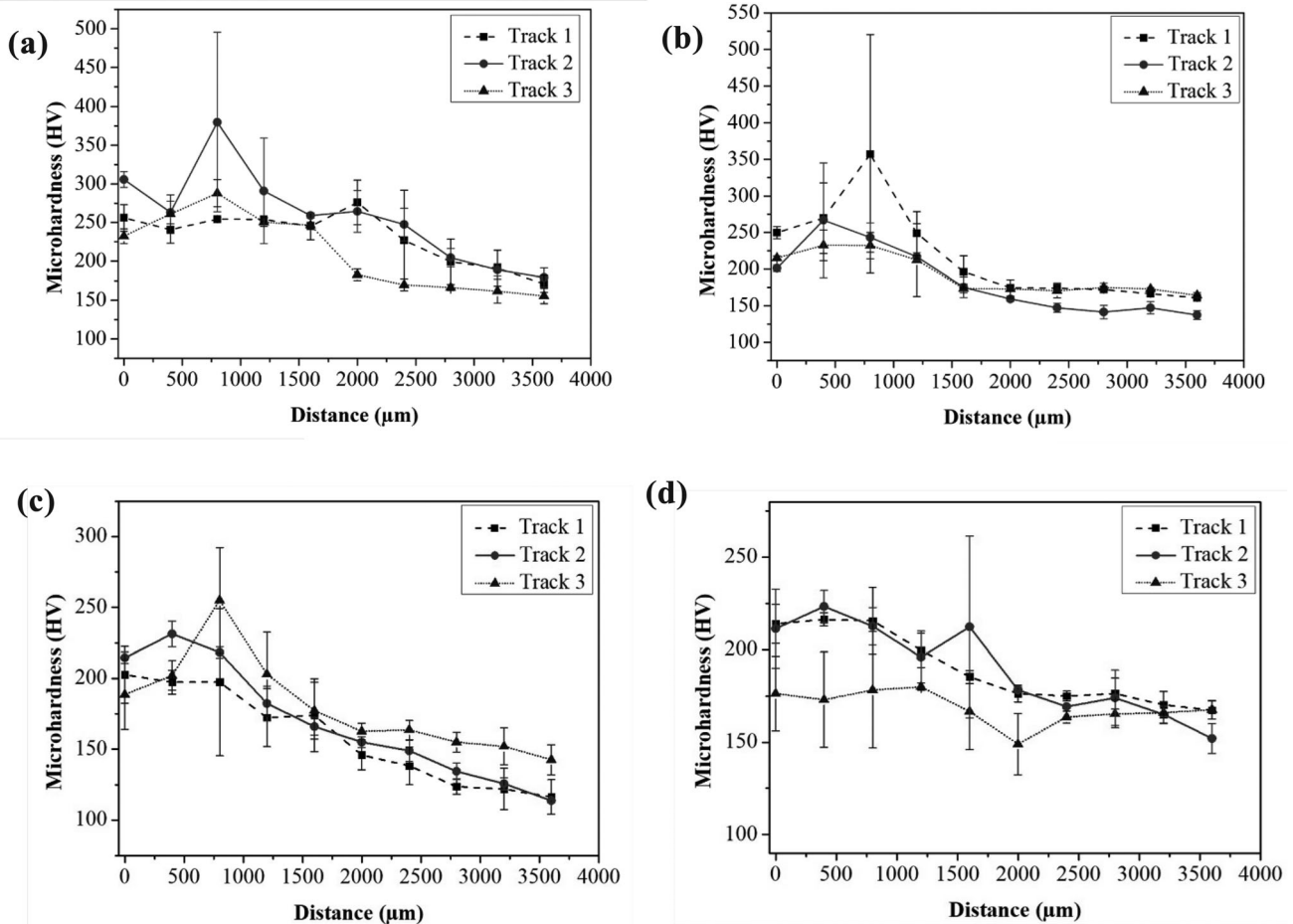


Figure 6. Results of microhardness mapping along the bead and substrate, showing the decrease in microhardness from the top of the bead to substrate for the energy densities (a) 20, (b) 24, (c) 28 and (d) 32 J/mm³.

all experiments. The temperature should be enough for the deposition of the material using the laser to achieve improved depositional resolution.

3.3 Microstructure analysis

The surface images of deposited tracks were taken using a high-definition camera after cleaning with ethanol, as shown in figure 2(a). The single track shape becomes more uniform as energy density increases in trials. Figure 5(a) presents the micrograph images of the deposited bead. It shows that beads are free from significant level defects, cracks, and other visual defects. It depicts elongated grains grown in the direction of the substrate plane, in the direction of conduction. The elongated grains were observed at the top of the beads. The variation in the microhardness from bead to substrate confirms the change in grain size. The micrographs also show the microstructural changes in all experimental conditions as the laser provides different heat for melting.

The penetration depth keeps increasing, and elongated grains are reducing with the increase in energy density. The temperature difference was confirmed by the temperature study discussed above. The interface between the substrate and HAZ of etched samples is presented in figure 5(b). The grain size was measured using ImageJ software. The average area grain size in the HAZ region is 3.65, 3.69, 3.86, and 4.03 μm for 20, 24, 28, and 32 J/mm³ energy density, respectively. It was observed that the effect of the energy density on single track characteristics is summarized as follows. It can be depicted that increasing the energy density at constant laser speed and wire feed rate can also show single track deposition ability. Low energy density shows the material's balling effect on the substrate's surface with a minimum penetration of the melt pool into the substrate.

3.4 Microhardness

Microhardness measurement results shown in figure 6 reveal a non-uniform microhardness distribution along the

height of the deposited bead. The microhardness significantly changes up to 1500 μm distance from the bead top to the substrate. This may be because of martensite formation due to variations in temperature gradient at different laser energy densities. By comparing the microhardness of the subsequent tracks, energy density was attributed to elongated grain generation. Using laser energy density and other process conditions in this study resulted in inhomogeneous elongated grain structures throughout the beads leading to a gradient in microhardness values. As discussed above, the grains were gradually refined with increased heat input, bringing more grain boundaries [26]. Consequently, the microhardness increased with energy density. The substrate region's lower area remained almost unchanged because of the absence of multiple thermal cycles during the LW-DED process.

4. Conclusions

This study focuses on depositing ER70S-6 wire on regular mild steel substrate using an in-house developed LW-DED experimental setup. It reveals the effect of different laser energy densities on bead characteristics such as aspect ratio, microstructure, porosity, and microhardness. The increase in energy density up to 32 J/mm^3 shows a high aspect ratio in bead geometry to build bulk parts with complex geometries further. This study observed lower penetration depth at lower laser energy density. The porosity results of single track deposition may help to estimate laser energy density for thin-walled samples. The temperature of the melt pool affects the process capability and forming bead morphology with a high aspect ratio. The laser spot diameter ensures proper wire melting and better interaction with the substrate. Higher hardness values were observed up to the deposited bead area.

Further, this study can be extended by introducing new deposition strategies and methods such as lowering wire diameters, modifying toolpath, and using pulsed lasers to build thin-walled parts. The LW-DED experimental setup used in this study can introduce different strategies and methods for extended studies.

Abbreviations

ρ_{sample}	Density of deposited track (g/cm^3)
ρ_{fluid}	Density of fluid (g/cm^3)
ρ_{air}	Density of air (g/cm^3)
M_{air}	Mass of sample in air (g)
M_{fluid}	Mass of sample in fluid (g)
Sp1	Spot 1
AM	Additive manufacturing
HAZ	Heat affected zone
LW-DED	Laser-wire feed directed energy deposition

Acknowledgements

The laser system used for this study was established through grant received from the Department of Science and Technology (DST), Government of India under Project Number DST/TDT/AMT/2017/026.

Availability of data and materials The corresponding author can provide the data from the paper upon reasonable request.

Declarations

Conflict of interest The authors declare that they have no known conflicts of interests.

References

- [1] Bastin A and Huang X 2022 Progress of additive manufacturing technology and its medical applications. *ASME Open J. Eng.* 1: 010802
- [2] Srivastava M, Rathee S, Patel V, Kumar A and Koppad P G 2022 A review of various materials for additive manufacturing: recent trends and processing issues. *J. Mater. Res. Technol.* 21: 2612–2641
- [3] Syed W U H and Li L 2005 Effects of wire feeding direction and location in multiple layer diode laser direct metal deposition. *Appl. Surf. Sci.* 248: 518–524
- [4] Rathor S, Kant R and Singla E 2023 Introduction to additive manufacturing: concepts, challenges, and future scope. *Industry 4.0: Concepts, Processes and System.* eds Ravi Kant Hema Gurung. Boca Raton. CRC Press. 192–217
- [5] Rathor S, Kumar S, Singla E, Kant R and Nirala C K 2023 Robotic tool-path generation for complex and overhang-angled parts through offline programming. In: *AIR '23: Proceedings of the 2023 6th International Conference on Advances in Robotics*, pp. 1–5
- [6] Oh W J, Lee W J, Kim M S, Jeon J B and Shim D S 2019 Repairing additive-manufactured 316L stainless steel using direct energy deposition. *Opt. Laser Technol.* 117: 6–17
- [7] Barr C, Abdul R, Rashid R, Palanisamy S, Watts J and Brandt M 2023 Examination of steel compatibility with additive manufacturing and repair via laser directed energy deposition. *J. Laser Appl.* 35: 022015
- [8] Matthes S, Kluge M, Jahn S and Emmelmann C 2020 Factors influencing powder-properties of TiAl6V4 along the L-PBF process chain. *Prog. Addit. Manuf.* 5: 33–39
- [9] Ahn D G 2021 Directed energy deposition DED process: state of the art. *Int. J. Precis. Eng. Manuf. Green Technol.* 8:2 8:703–742
- [10] Svetlizky D, Zheng B, Vyatskikh A, Das M, Bose S, Bandyopadhyay A, Schoenung J M, Lavernia E J and Eliaz N 2022 Laser-based directed energy deposition (DED-LB) of advanced materials. *Mater. Sci. Eng. A* 840: 142967
- [11] Toyserkani E, Sarker D, Ibadode O O, Liravi F, Russo P and Taherkhani K 2021 Directed energy deposition (DED). *Metal Additive Manufacturing*. John Wiley & Sons, Ltd. 137–202

- [12] Akbari M, Ding Y and Kovacevic R 2017 Process development for a robotized laser wire additive manufacturing. In: *ASME 2017 12th International Manufacturing Science and Engineering Conference*.50732
- [13] Garmendia I, Pujana J, Lamikiz A, Flores J and Madarieta M 2019 Development of an intra-layer adaptive toolpath generation control procedure in the laser metal wire deposition process. *Materials*. 12: 352
- [14] Oliari S H, Monteiro D'Oliveira A S C and Schulz M 2017 Additive manufacturing of H11 with wire-based laser metal deposition. *Soldagem & Inspeção*. 22: 466–479
- [15] Metzbowyer E A 1981 Laser welding. *Naval Eng. J.* 93: 49–58
- [16] Zhang Y, Lan L and Shi Q 2023 Correlation between weld metal microstructure evolution and welding process parameters of low alloy ferritic steel weldments. *Steel Res. Int.* 94: 2200797
- [17] Uralde V, Suarez A, Aldalur E, Veiga F and Ballesteros T 2022 Wall fabrication by direct energy deposition (DED) combining mild steel (ER70) and stainless steel (SS 316L): microstructure and mechanical properties. *Materials*. 15: 1–13
- [18] Spierings A B, Schneider M and Eggenberger R 2011 Comparison of density measurement techniques for additive manufactured metallic parts. *Rapid Prototyp. J.* 17: 380–386
- [19] Shaikh M O, Chen C C, Chiang H C, Chen J R, Chou Y C, Kuo T Y, Ameyama K and Chuang C H 2020 Additive manufacturing using fine wire-based laser metal deposition. *Rapid Prototyp. J.* 26: 473–483
- [20] Shah K, Pinkerton A J, Salman A and Li L 2010 Effects of melt pool variables and process parameters in laser direct metal deposition of aerospace alloys. *Mater. Manuf. Process*. 25: 1372–1380
- [21] Zhou J and Tsai H L 2013 Melt Flow and Mass Transfer in Hybrid Laser-GMA Welding of 304 Stainless Steels. American Society of Mechanical Engineers, Fluids Engineering Division (Publication) FEDSM, p 55560
- [22] Zhang D, Wei Y, Zhan X, Chen J, Li H and Wang Y 2018 Numerical simulation of keyhole behaviors and droplet transfer in laser-MIG hybrid welding of Invar alloy. *Int. J. Numer. Methods Heat Fluid Flow*. 28: 1974–1993
- [23] Steiner M F, Speier M, Kelbassa J, Schopphoven T and Häfner C L 2022 Influence of tool path planning on process stability and deposition accuracy in laser material deposition with coaxial wire feed. *J. Laser Appl.* 34: 012026
- [24] Dass A and Moridi A 2019 State of the art in directed energy deposition: from additive manufacturing to materials design. *Coatings*. 9: 1–26
- [25] Yadav R, Yadav R and Kant R 2023 Experimental study on laser bending of mild steel with buckling mechanism. *Opt. Laser Technol.* 167: 109803
- [26] Yadav R and Kant R 2022 Effectiveness of forced cooling during laser bending of duplex-2205. *Mater. Manuf. Process*. 38: 598–607

Springer Nature or its licensor (e.g. a society or other partner) holds exclusive rights to this article under a publishing agreement with the author(s) or other rightsholder(s); author self-archiving of the accepted manuscript version of this article is solely governed by the terms of such publishing agreement and applicable law.